

Synthesis and Redox Behavior of Nanocrystalline Hausmannite (Mn₃O₄)

Jenna Pike,[†] Jonathan Hanson,[‡] Lihua Zhang,[§] and Siu-Wai Chan^{*,†}

Department of Applied Physics and Applied Mathematics, Columbia University, 200 Mudd Building, 500 West 120th Street, New York, New York 10027, Chemistry Department, Brookhaven National Laboratory, Upton, New York 11973-5000, and Center for Functional Nanomaterials, Brookhaven National Laboratory, Upton, New York 11973-5000

Received June 26, 2007. Revised Manuscript Received September 8, 2007

Hausmannite (Mn₃O₄) nanoparticles have been prepared by mixing aqueous solutions of manganese nitrate and hexamethylenetetramine from 20 to 80 °C. Activation energy for the particle formation increases from 0.5 to 0.8 kJ/mol with nitrate concentration. Nanoparticles (18–41 nm) with a faceted structure are prepared by this method. We describe synchrotron in-situ time-resolved XRD experiments in which Mn₃O₄ nanoparticles are reduced to MnO and subsequently reoxidized in ramping temperature conditions. The temperature of Mn₃O₄ to MnO reduction decreases as Mn₃O₄ particle size decreases. On oxidation, 18 nm and smaller MnO nanoparticles formed the intermediate phase Mn₅O₈ (MnO → Mn₃O₄ → Mn₅O₈ → Mn₂O₃), while larger MnO particles oxidized to Mn₃O₄ then directly to Mn₂O₃. Formation of Mn₃O₄ occurred at lower temperature for smaller MnO nanoparticles. Further oxidation to Mn₂O₃ required higher temperatures for the initially smaller MnO nanoparticles, indicating that the kinetics of forming the new oxide phases is not controlled by diffusion, where smaller distance favors faster reaction, but by nucleation barrier.

1. Introduction

Manganese is the tenth most abundant element in the earth's crust¹ and occurs in nature in the +2, +3, and +4 oxidation states. Manganese oxides are commonly used in a wide range of applications including dry-cell batteries,² pigments,¹ catalysts,^{3–7} and water-purifying agents.¹ The greatest percentage of the world's manganese production is consumed in steel production, where it is added for increased strength.¹ Manganese oxides are active catalysts in several oxidation and reduction reactions, including oxidation of methane and carbon monoxide and selective reduction of nitrobenzene.⁸ Chang and McCarty found the oxygen absorption and desorption behavior of manganese oxide as an

oxygen storage component to be superior to that of cerium oxide.⁹ Manganese forms the stable oxides MnO, α-Mn₃O₄, α-Mn₂O₃, and β-MnO₂ as well as the metastable Mn₅O₈. The structural properties of these oxides are listed in Table 1. Reduction and oxidation of manganese oxides are reversible up to Mn₂O₃; formation of MnO₂ in pure oxygen requires pressures greater than 3000 bar.¹

The manganese oxide hausmannite is a black mineral that forms the spinel structure with tetragonal distortion due to a Jahn–Teller effect on Mn⁺². In the Mn⁺²(Mn⁺³)₂O₄ structure the Mn⁺² and Mn⁺³ ions occupy the tetrahedral and octahedral sites, respectively.¹⁰ Mn₃O₄ is ferromagnetic below 43 K.¹¹ Hausmannite has been shown to be an active catalyst for reduction of nitrobenzene to nitrosobenzene,³ decomposition of NO_x,⁸ and oxidation of methane and carbon monoxide.⁸ Hausmannite has a tetragonal crystal structure with lattice parameters $a = b = 5.762 \text{ \AA}$ and $c = 9.4696 \text{ \AA}$ and space group $I4_1/amd$.

Nanocrystalline Mn₃O₄ has been synthesized by a number of methods that produce relatively monodisperse particles and rods. Solvothermal methods have resulted in 9–15¹² and 50 nm Mn₃O₄ particles,¹³ microwave irradiation of KMnO₄

* To whom correspondence should be addressed. Phone: 212-854-8519. Fax: 212-854-8257. E-mail: sc174@columbia.edu.

[†] Columbia University.

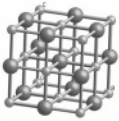
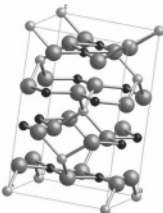
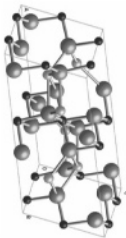
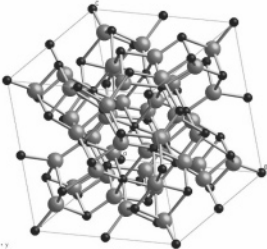
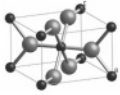
[‡] Chemistry Department, Brookhaven National Laboratory.

[§] Center for Functional Nanomaterials, Brookhaven National Laboratory.

- (1) Post, J. Manganese oxide minerals: crystal structures and economic and environmental significance. *Proc. Natl. Acad. Sci. U.S.A.* **1999**, *96* (7), 3447–3454.
- (2) Thackeray, M. M. Manganese oxides for lithium batteries. *Prog. Solid State Chem.* **1997**, *25*, 1–71.
- (3) Maltha, A.; Favre, T. L. F.; Kist, H. F.; Zuur, A. P.; Ponec, V. Manganese oxides as catalysts for the selective reduction of nitrobenzene to nitrosobenzene. *J. Catal.* **1994**, *149*, 364–374.
- (4) Baldi, M.; Finocchio, E.; Milella, F.; Busca, G. Catalytic combustion of C3 hydrocarbons and oxygenates over Mn₃O₄. *Appl. Catal. B: Environ.* **1998**, *16*, 43–51.
- (5) Yamashita, T.; Vannice, A. Temperature-programmed desorption of NO adsorbed on Mn₂O₃ and Mn₃O₄. *Appl. Catal. B: Environ.* **1997**, *13*, 141–155.
- (6) Baldi, M.; Finocchio, E.; Pistarino, C.; Busca, G. Evaluation of the mechanism of the oxy-dehydration of propane over manganese oxide. *Appl. Catal. A* **1998**, *173*, 61–74.
- (7) Te, M.; Foley, H. C. Intrinsic reactivities of manganese oxides for carbon monoxide hydrogenation catalysis. *Appl. Catal. A* **1994**, *119*, 97–106.

- (8) Stobbe, E. R.; Boer, B. A. d.; Geus, J. W. The reduction and oxidation behavior of manganese oxides. *Catal. Today* **1999**, *47*, 161–167.
- (9) Chang, Y.-f.; McCarty, J. G. Novel oxygen storage components for advanced catalysis for emission control in natural gas fueled vehicles. *Catal. Today* **1996**, *30*, 163–170.
- (10) Greenwood, N. N.; Earnshaw, A. *Chemistry of the Elements*; Pergamon Press: New York, 1984.
- (11) Boucher, B.; Buhl, R.; Perrin, M. Magnetic structure of Mn₃O₄ by neutron diffraction. *J. Appl. Phys.* **1971**, *42* (4), 1615–1617.
- (12) Weixin, Z.; Cheng, W.; Xiaoming, Z.; Yi, X.; Yitai, Q. Low temperature synthesis of nanocrystalline Mn₃O₄ by a solvothermal method. *Solid State Ionics* **1999**, *117*, 331–335.

Table 1. Manganese Oxides Structural Data

Oxide	MnO	α -Mn ₃ O ₄	Mn ₅ O ₈	α -Mn ₂ O ₃	β -MnO ₂
JCPDS	71-1177	24-0734	39-1218	41-1442	43-1455
Mineral Name	Manganosite	Hausmannite	n/a	Bixbyite	pyrolusite
Valence	+2	+2, +3	+2, +4	+3	+4
Crystal Structure	Cubic	Tetragonal	Monoclinic	Cubic	Tetragonal/ rutile
Space group	Fm $\bar{3}$ m	I4 ₁ /amd	C2/m	Ia $\bar{3}$	P4 ₁ /mnm
Lattice Parameter (Å)	a = 4.446	a = 5.7621 c = 9.4696	a = 10.392, b = 5.730 c = 4.866, β = 109.62	a = 9.4091	a = 4.3999 c = 2.8740
Unit Cell Model					
Formula units/unit cell	4	4	4	16	2

dissolved in ethanol produced 30 nm Mn₃O₄ particles,¹⁴ thermal evaporation of Mn powders resulted in 42 nm Mn₃O₄ particles,¹⁵ and thermal decomposition of manganese oxalate in N₂ produced 100 nm Mn₃O₄ particles.¹⁶ Formation of Mn₃O₄ nanorods has also been reported: single-crystal nanowires 40–80 nm wide and up to 150 μ m long by molten salt synthesis¹⁷ and 6 nm by 17 nm rods by dissolution of manganese(II) acetate and an amide in water at room temperature.¹⁸

Metastable Mn₅O₈ has been observed to form by oxidation of Mn₃O₄ at 723 K in air¹⁹ by reacting manganese nitrate and sodium hydroxide²⁰ and from oxidation of 32 nm Mn₃O₄ particles.²¹ In the latter study oxidation of lower surface area

Mn₃O₄ particles and heating rates of 600 °C resulted in formation of Mn₂O₃ particles rather than Mn₅O₈.²¹ Previous studies on formation of Mn₅O₈ have not offered an explanation for formation of this phase.

The aim of the present work is 2-fold: to prepare Mn₃O₄ nanoparticles by low-temperature aqueous synthesis and characterize the products resulting from reduction of nanoscale Mn₃O₄ in 5% CO/He and oxidation of nanoscale MnO in 100% O₂. We use in-situ time-resolved X-ray diffraction (TR-XRD) to monitor formation of reduction and oxidation products. The combination of high-intensity synchrotron radiation and rapid data collection devices allows for detection of phase changes during the reaction in real time and with great sensitivity. To the best of our knowledge, no systematic studies using in-situ XRD and synchrotron radiation have been reported for reduction of nanoscale Mn₃O₄ by CO gas or oxidation of MnO using pure oxygen. Such studies are important in determining reduction and oxidation profiles in manganese oxides as a function of nanoparticle size and in developing a fundamental understanding of the manganese oxide nanoparticle system in catalytic operating conditions.

2. Experimental Procedure

2.1. Nanoparticle Synthesis. Mn₃O₄ nanoparticles were prepared from aqueous solutions of manganese nitrate hydrate Mn(NO₃)₂·

- (13) Zhang, W.; Yang, Z.; Liu, Y.; Tang, S.; Han, X.; Chen, M. Controlled synthesis of Mn₃O₄ nanocrystallites and MnOOH nanorods by a solvothermal method. *J. Cryst. Growth* **2004**, *263*, 394–399.
- (14) Bousquet-Berthelin, C.; Stuerger, D. Flash microwave synthesis of Mn₃O₄-hausmannite nanoparticles. *J. Mater. Sci.* **2005**, *40*, 253–255.
- (15) Chang, Y. Q.; Xu, X. Y.; Luo, X. H.; Chen, C. P.; Yu, D. P. Synthesis and characterization of Mn₃O₄ nanoparticles. *J. Cryst. Growth* **2004**, *264*, 232–236.
- (16) Ahmad, T.; Ramanujachary, K. V.; Lofland, S. E.; Ganguli, A. K. Nanorods of manganese oxalate: a single source precursor to different manganese oxides nanoparticles (MnO, Mn₂O₃, Mn₃O₄). *J. Mater. Chem.* **2004**, *14*, 3406–3410.
- (17) Wang, W.; Xu, C.; Wang, G.; Liu, Y.; Zheng, C. Preparation of smooth single-crystal Mn₃O₄ nanowires. *Adv. Mater.* **2002**, *14* (11), 837–840.
- (18) Vázquez-Olmos, A.; Redón, R.; Rodríguez-Gattorno, G.; Mata-Zamora, M. E.; Morales-Leal, F.; Fernández-Osorio, A. L.; Saniger, J. M. One-step synthesis of Mn₃O₄ nanoparticles: structural and magnetic study. *J. Colloid Interface Sci.* **2005**, *291*, 175–180.
- (19) Azzoni, C. B.; Mozzati, M. C.; Galinetto, P.; Paleari, A.; Massorotti, V.; Capsoni, D.; Bini, M. Thermal stability and structural transition of metastable Mn₅O₈: in situ micro-Raman study. *Solid State Commun.* **1999**, *112*, 375–378.

- (20) Punnoose, A.; Magnone, H.; Seehra, M. S. Synthesis and antiferromagnetism of Mn₅O₈. *IEEE Trans. Magn.* **2001**, *37* (4), 2150–2152.
- (21) Gillot, B.; Guendouzi, M. E.; Laarj, M. Particle size effects on the oxidation-reduction behavior of Mn₃O₄ hausmannite. *Mater. Chem. Phys.* **2001**, *70*, 54–60.

$x\text{H}_2\text{O}$ (99.98% purity, Alfa Aesar) and hexamethylenetetramine ($\text{C}_6\text{H}_{12}\text{N}_4$) (99+% purity, Alfa Aesar). Two methods were used in the synthesis of Mn_3O_4 . In the first method (standard method) the two chemicals are mixed separately with equal quantities of ultrapure water to concentrations of 0.02 and 0.1 M $\text{Mn}(\text{NO}_3)_2$ solution and 0.5 M hexamethylenetetramine (HMT) solution. The separate solutions were stirred for 30 min and then combined and heated using a water-jacketed beaker connected to a heating circulator (ThermoElectric Corp. Neslab EX10) to synthesis temperatures ranging from 22 to 80 °C for 30 min to 4 h. In the second method (injection method) the same mass of HMT used in the standard method was dissolved into the total quantity of ultrapure water and stirred for 30 min at the synthesis temperature. The mass of manganese nitrate used in the standard method was dissolved into 5 mL of ultrapure water and injected into the HMT solution after 30 min of stirring. In both cases the particles were harvested by filtering the solution through a 0.22 μm microcellulose filter using an aspirator. The particles were rinsed with ultrapure water to remove HMT and allowed to dry in air.

Intermediate-sized Mn_3O_4 nanoparticles were synthesized by calcining manganese nitrate in air at 1050 °C for 0.5, 2, and 6 h. Micrometer-sized Mn_3O_4 was synthesized by calcining manganese nitrate in air at 1050 °C for 12 h.

2.2. Particle Characterization. Transmission electron microscopy (TEM) samples were prepared by extracting a small amount of the metal oxide nanoparticle–HMT solution, diluting with water, and adding several drops of isopropyl alcohol. A copper grid covered by a carbon film was then dipped into the diluted solution and allowed to dry in air. Shape, size, and size distribution of nanoparticles were examined by TEM (JEM 100C). High-resolution TEM (HR-TEM) samples were prepared by the same preparation technique on a copper grid covered with lacey carbon film and examined using a JEOL 4000EX TEM. HR-TEM work was performed at Brookhaven National Laboratory using facilities at the Center for Functional Nanomaterials.

X-ray diffraction (XRD) measurements were taken of the dried powders using a Scintag X2 diffractometer with a $\text{Cu K}\alpha$ anode to verify the phase purity of the products at a scan rate of 0.02°/step and 5 s/step. Crystallite size was calculated by fitting the synchrotron XRD results using the Scherrer equation, $d = 0.941\lambda / (B \cos \theta_B)$, where λ is the wavelength, B is the full width at half-maximum (FWHM) of the peak, and θ_B is the Bragg angle. A correction was made for instrumental peak broadening using the corresponding peaks in micrometer-sized powder. The crystallite sizes measured from the four peaks (112), (103), (211), and (224) were averaged to obtain the Mn_3O_4 crystallite size, and the spreads among sizes from different peaks were expressed as error bars.

The particle size of the intermediate and bulk Mn_3O_4 samples was measured from SEM using a JEOL 5600LV instrument.

2.3. Redox with in-Situ XRD. Time-resolved XRD (TR-XRD) data were collected at beamline X7B at the National Synchrotron Light Source at Brookhaven National Lab ($\lambda = 0.922 \text{ \AA}$). Diffraction patterns were collected using a MAR345 area detector at 3 min intervals. The loose powders were loaded into an open sapphire capillary with an inner diameter of 0.5 mm. Quartz wool was inserted into each end to secure the sample position while gas flowed. One end of the capillary was connected to a gas inlet, while the other end was connected to a flow meter. A flow rate of about 15 cm^3/min was maintained throughout the process. The powder was heated using a Kanthal wire that wrapped around the capillary. A thermocouple was inserted directly into the capillary near the sample to maintain accurate temperature during the XRD measurements.

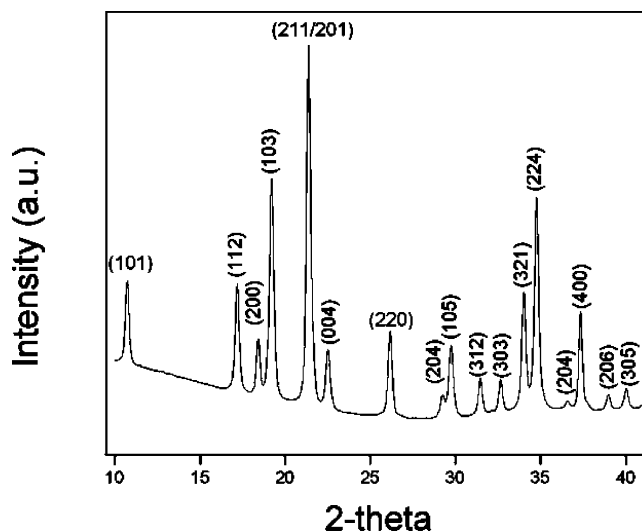


Figure 1. Synchrotron XRD pattern of Mn_3O_4 from nitrate-HMT synthesis.

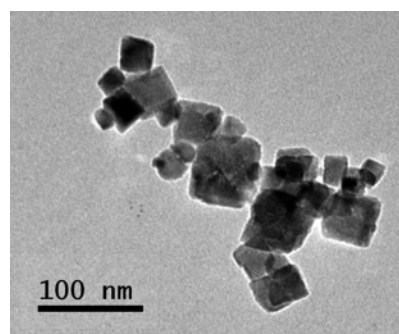


Figure 2. TEM image of Mn_3O_4 nanoparticles prepared from 0.1 M $\text{Mn}(\text{NO}_3)_2$ and 0.5 M HMT at 50 °C for 150 min.

Reduction and oxidation experiments were conducted using a constant heating rate of 400 °C/h up to 800 °C. For reduction experiments, a gas mixture of 5% CO/He (99.99% purity) was used to reduce Mn_3O_4 powders to MnO . After reduction, MnO samples were reoxidized by heating at 400 °C/h in 100% O_2 . Oxidation experiments were also conducted on bulk MnO powders using a heating rate of 400 °C/h in 100% O_2 .

3. Results

3.1. Synthesis. The initially clear, colorless HMT–nitrate solution changes within several minutes to a light orange color and gradually becomes darker orange-brown and cloudy as the reaction proceeds. XRD shows that the product is Mn_3O_4 with no other phases present, as shown in Figure 1. The sample presented in Figure 1 was prepared using a manganese nitrate concentration of 0.1 M at 80 °C, synthesized for 50 min. The method of synthesis, standard or injection, did not result in any apparent difference in the purity, size, size distribution, or morphology of the product.

Manganese oxide nanoparticles sizes range from 18–41 nm as calculated from XRD depending on synthesis conditions (reaction time, manganese nitrate concentration, and synthesis temperature). Crystallite size measured from XRD was at the lower end of the particle-size range measured from TEM. This is expected as the XRD measurement represents a weighted mean of the actual crystallite sizes. Throughout this paper we use the term particle size to refer to the

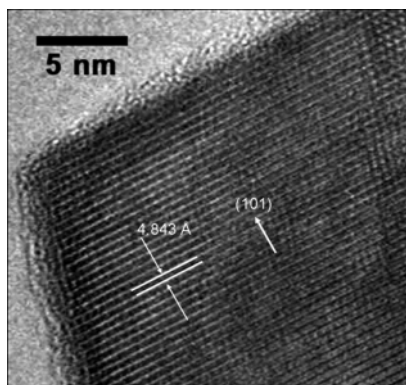


Figure 3. HR-TEM image of Mn_3O_4 prepared from 0.02 M $\text{Mn}(\text{NO}_3)_2$ and 0.5 M HMT at 40 °C for 50 min.

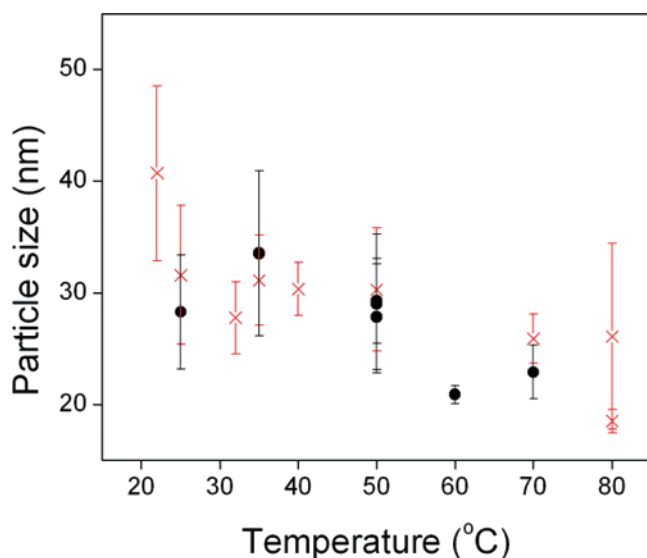


Figure 4. Mn_3O_4 nanoparticle size as a function of reaction temperature: (● and ×) 0.02 and 0.1 M $\text{Mn}(\text{NO}_3)_2$, respectively. Synthesis time ranges from 30 to 240 min.

crystallite size measured using XRD. Figure 2 is a TEM image of Mn_3O_4 synthesized using 0.02 M $\text{Mn}(\text{NO}_3)_2$ at 50 °C for 60 min. From XRD this sample had a particle size of 29 ± 6 nm, while the particle size measured from TEM ranged from 25 to 100 nm. Particle morphology varied within each sample, as shown in Figure 2. Individual Mn_3O_4 nanoparticles observed in TEM by tilting the specimen showed complex faceted structures.

High-resolution TEM images show that the particles are highly crystalline (Figure 3) with a thin amorphous layer surrounding each particle that was observed to disappear over several minutes with the beam focused on the sample.

Particles were observed to grow as the reaction time increased but reached a maximum size after several hours. Nitrate concentration did not show a significant effect on particle size. Of the reaction variables, synthesis temperature had the greatest effect on Mn_3O_4 nanoparticle size, as shown in Figure 4, which includes particles made from 0.02 and 0.1 M manganese nitrate and with reaction times ranging from 30 to 240 min. Particles made from 0.1 M $\text{Mn}(\text{NO}_3)_2$ and harvested after 150 min were 28 ± 3 nm when synthesized at 35 °C and 41 ± 8 nm when synthesized at 22 °C.

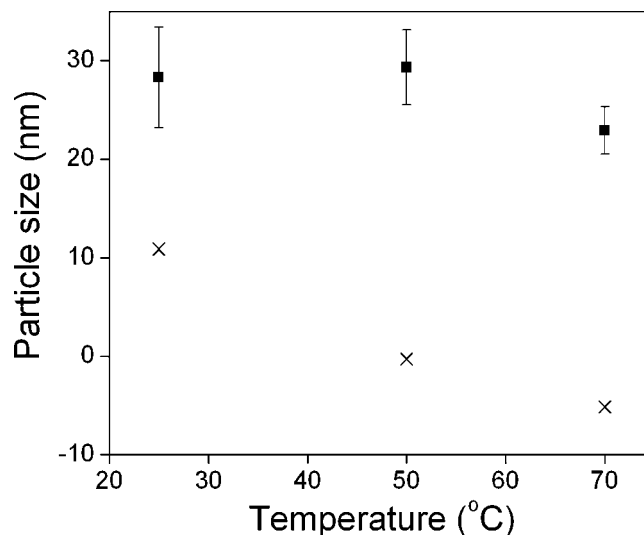


Figure 5. Mn_3O_4 particle size as a function of synthesis temperature from 0.02 M $\text{Mn}(\text{NO}_3)_2$ and reaction time of 150 min. (■) Average particle size obtained by XRD. (×) Size difference as determined from peaks (004) and (220).

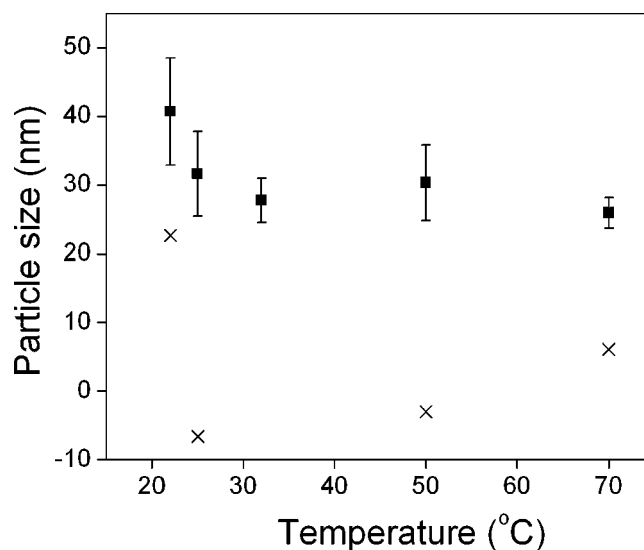


Figure 6. Mn_3O_4 particle size as a function of synthesis temperature from 0.1 M $\text{Mn}(\text{NO}_3)_2$ and reaction time of 150 min. (■) Average particle size obtained by XRD. (×) Size difference as determined from peaks (004) and (220).

A study of Mn_3O_4 nanoparticles synthesized at temperatures ranging from 22 to 70 °C for 150 min also showed a decrease in median particle size with an increase in synthesis temperature, as shown by the solid symbols in Figures 5 and 6 using 0.02 and 0.1 M $\text{Mn}(\text{NO}_3)_2$, respectively. The largest Mn_3O_4 nanoparticles formed were 41 nm, from 0.1 M $\text{Mn}(\text{NO}_3)_2$ at 22 °C for 150 min. The smallest Mn_3O_4 nanoparticles, at 23 ± 2 nm, were formed using 0.02 M $\text{Mn}(\text{NO}_3)_2$ at 70 °C. No particles were formed after 150 min with a reaction temperature of 10 °C and manganese nitrate concentration of 0.1 M.

In general, the spread in the Mn_3O_4 nanoparticle size measurement decreases with increasing synthesis temperature, as illustrated by the error bars in Figures 5 and 6. Particle size difference for the set of samples synthesized at 150 min over a range of temperatures was determined by calculating the absolute value of crystallite size obtained from

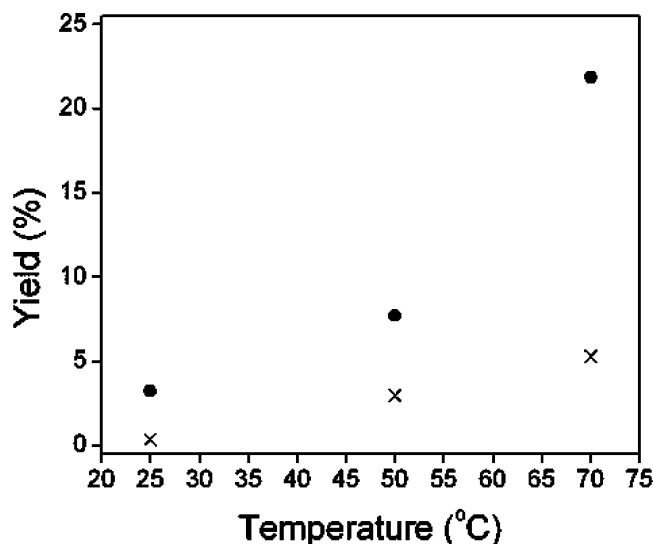


Figure 7. Yield of Mn_3O_4 synthesis by the aqueous HMT-nitrate method using 0.5 M HMT and 150 min: (● and ×) 0.02 and 0.1 M $\text{Mn}(\text{NO}_3)_2$, respectively.

the (004) peak subtracted from that of the (220) peak and is identified by × in Figures 5 and 6. Anisotropy decreases initially as the synthesis temperature increases with the most equiaxed particles forming at 50 °C for both 0.02 and 0.1 M $\text{Mn}(\text{NO}_3)_2$ concentrations.

The higher $\text{Mn}(\text{NO}_3)_2$ concentration (0.1 M) resulted in a lower relative yield compared to the 0.02 M $\text{Mn}(\text{NO}_3)_2$ reactions. Yield, in terms of percent of theoretical yield, is shown in Figure 7. Theoretical yield is calculated as the total mass of Mn_3O_4 that would result if all manganese ions present in $\text{Mn}(\text{NO}_3)_2$ reacted to form Mn_3O_4 . In terms of mass of Mn_3O_4 powder, the amount of product obtained from the higher nitrate concentration condition was approximately double that obtained from the lower concentration. The yield increases as reaction temperature increases.

Activation energy (E_a) for the reaction is calculated using the Arrhenius relationship, $r = A \exp(-E_a/RT)$, where r is the rate, R is the ideal gas constant (8.314 J/mol K), and temperature is T . In Figure 8 the reaction rate, calculated as the yield per unit time, is plotted against $1000/T$. The slope of the linear fit is used to determine E_a for formation of Mn_3O_4 nanoparticles from 0.1 and 0.02 M $\text{Mn}(\text{NO}_3)_2$ using 0.5 M HMT and a reaction time of 150 min. Activation energy is 768 J/mol (7.96 meV) for 0.1 M $\text{Mn}(\text{NO}_3)_2$ and 514 J/mol (5.33 meV) for 0.02 M $\text{Mn}(\text{NO}_3)_2$.

Larger manganese oxide particles obtained by calcining $\text{Mn}(\text{NO}_3)_2$ in air at 1050 °C for 0.5, 2, and 6 h were measured by XRD to be 160, 265, and 345 nm, respectively.

3.2. Mn_3O_4 Reduction. During in-situ TR-XRD experiments in 5% CO/He gas Mn_3O_4 particles reduce to MnO. Reduction temperature is observed to decrease as initial Mn_3O_4 particle size decreases, as shown in Figure 9. The dashed lines are included to guide the eye. The dashed lines connect temperatures at which MnO is initially observed in reducing Mn_3O_4 nanoparticles of specific initial sizes (■) and the temperature of complete reduction of Mn_3O_4 to MnO (□). Smaller Mn_3O_4 nanoparticles reduce to MnO at lower temperature than larger nanoparticles and bulk Mn_3O_4 . The smallest Mn_3O_4 particles evaluated, 16 nm, began to form

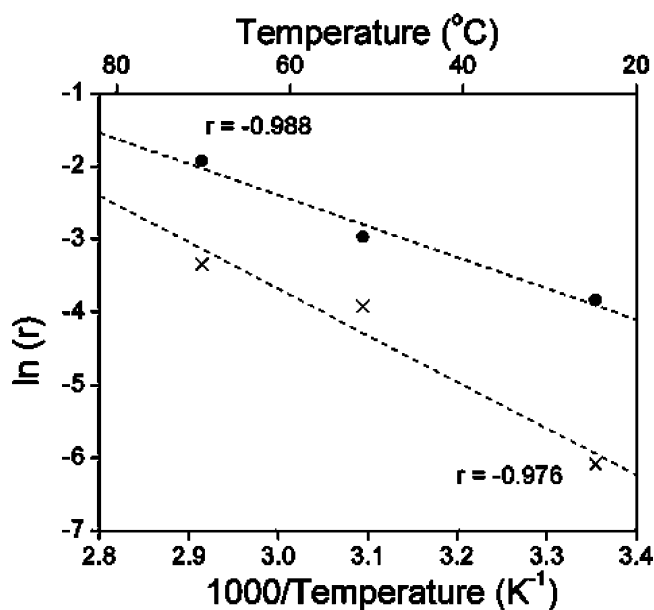


Figure 8. Activation energy for formation of Mn_3O_4 calculated using the rate in terms of yield per time: (● and ×) 0.02 and 0.1 M $\text{Mn}(\text{NO}_3)_2$, respectively.

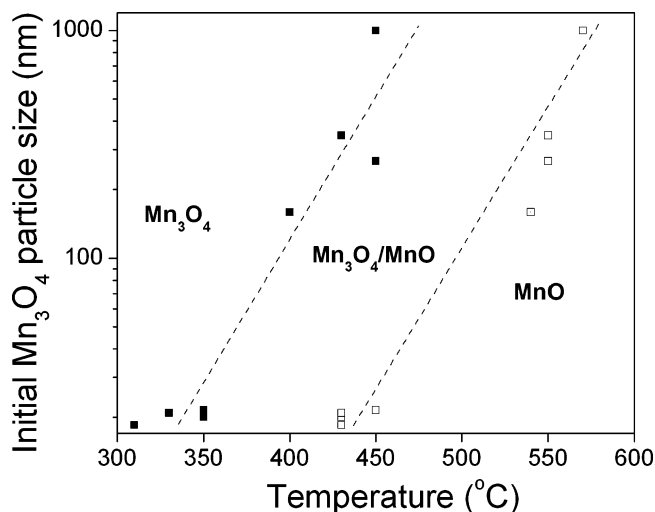


Figure 9. Mn_3O_4 nanoparticles reduce to MnO in 5% CO/He gas: (■) formation of MnO; (□) complete reduction of Mn_3O_4 to MnO.

MnO at 310 °C, while bulk Mn_3O_4 began reduction to MnO at 450 °C. Full reduction to MnO was completed at about 430–450 °C for the approximately 20 nm Mn_3O_4 particles; larger Mn_3O_4 particles required heating to 570 °C to reduce completely to MnO. The positive slopes of the dashed lines in Figure 9 illustrate the characteristic of nanoparticle systems to react more readily than bulk material due to faster kinetics and shorter diffusion distances.

Several of the bulk and nanoparticle samples examined were heated to 800 °C, and no further reduction was observed. MnO particles formed from reduction of Mn_3O_4 nanoparticles ranging in size from 14 to 18 nm with smaller Mn_3O_4 nanoparticles forming smaller MnO nanoparticles. MnO particles formed by reduction of bulk and nanoscale Mn_3O_4 exhibited the rock salt structure.

3.3. MnO Oxidation. MnO nanoparticles from reduced Mn_3O_4 nanoparticles were heated in 5% O_2 /He and 100% O_2 during TR-XRD experiments. No phase change was observed when 5% O_2 was used as the oxidizing gas. In

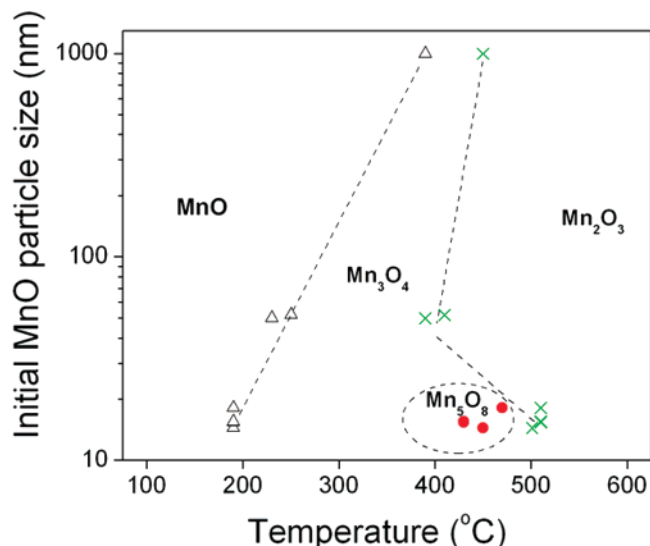


Figure 10. Phases formed from oxidation of MnO bulk- and nanoparticles in 100% O₂ gas. First indication by XRD of formation of (Δ) Mn₃O₄, (●) Mn₅O₈, and (×) Mn₂O₃.

100% O₂ oxidation environment the MnO nanoparticles smaller than 18 nm were observed to form Mn₃O₄, then Mn₅O₈, then Mn₂O₃. Larger MnO particles (50 nm and bulk MnO) oxidize to Mn₃O₄ and then directly to Mn₂O₃ with no trace of Mn₅O₈ formation. The temperatures at which Mn₃O₄, Mn₅O₈, and Mn₂O₃ are initially detected are presented in Figure 10, with dashed lines included to guide the eye. As in Figure 9, the positively sloped lines indicate that faster kinetics in the nanoscale is present in the oxidation process. A negative slope, as in formation of Mn₂O₃ from Mn₅O₈, indicates a barrier to nucleation of the oxidation product. The temperature at which Mn₃O₄ is first detected is indicated with Δ, the temperature of initial formation of Mn₅O₈ with ●, and the temperature at which Mn₂O₃ is first observed with ×.

Oxidation of nanoscale MnO (<50 nm) does not proceed in a simple stepwise fashion, with MnO oxidizing to form a two-phase mixture of MnO/Mn₃O₄, then becoming pure Mn₃O₄ with increasing temperature, and then forming Mn₃O₄/Mn₅O₈, etc. Rather, it was observed that trace MnO peaks remained visible even while more highly oxidized phases formed, and nearly all of the samples evaluated exhibited three phase regions. Figure 10 is a simplified view of the pathways observed in the oxidation of MnO in which only the initial formation of each phase is presented.

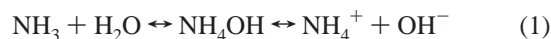
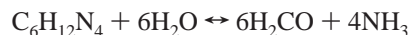
The temperature at which MnO begins to form Mn₃O₄ is observed to increase with increasing MnO particle size, similar to the results of Mn₃O₄ reduction experiments. Initially 14–18 nm MnO particles formed Mn₃O₄ at 190 °C, while oxidation to Mn₃O₄ was not apparent in the bulk MnO particles until the temperature reached 390 °C.

After formation of Mn₃O₄, the intermediate phase Mn₅O₈ forms from the initially 14–18 nm MnO particles in the 430–470 °C temperature range. Formation of Mn₂O₃ begins at approximately 510 °C in the initially 14–18 nm MnO nanoparticles, while the initially 50 nm MnO particles oxidized to Mn₂O₃ at 390–410 °C. The bulk MnO used in this study formed Mn₂O₃ at 450 °C.

4. Discussion

4.1. Synthesis. According to our previous work,²² HMT acts as an ammonia agent and a surfactant in the aqueous synthesis of ZnO nanoparticles. In contrast to the ZnO nanoparticle synthesis by this method, in which Zn(OH)₂ formed at lower temperatures, no manganese hydroxide phases were observed to form under the conditions studied. Also, in contrast to aqueous nitrate–HMT synthesis of ZnO and CuO²³ nanoparticles, Mn₃O₄ nanoparticles show a low aspect ratio rather than the ZnO nanorods or CuO nanowires formed. Low aspect ratio CeO₂ nanoparticles were also prepared by this method.²⁴ As anticipated for these four processes, shape isotropy increases as lattice symmetry increases: CeO₂ is cubic, Mn₃O₄ is tetragonal, ZnO is hexagonal, and CuO has a monoclinic structure.

Two explanations for the decrease in Mn₃O₄ particle size with increasing synthesis temperature are considered. It is suggested that nucleation is more active at higher temperatures, consuming manganese ions initially and limiting the number of ions available in the solution for subsequent growth of individual particles. Another factor may result from the effect of temperature on the decomposition of HMT in water, as given in reaction 1



HMT dissociates to ammonium and hydroxide ions in water. An increase in the concentration of OH[−] ions with temperature may result in more rapid hydrolysis of Mn⁺³ ions from dissociated Mn(NO₃)₂. The subsequent condensation of manganese hydroxide to form Mn₃O₄ would then take place in a solution depleted of manganese ions required for growth.

Average size is controlled by the synthesis conditions, although TEM shows a rather wide range of particle sizes in each batch, suggesting that nucleation does not occur in a single event but that particles are nucleated and grow throughout the initial synthesis process. It is possible that as the particles grow particular planes grow preferentially, which could explain the nonuniform morphology observed.

Use of standard and injection methods of synthesis did not result in an appreciable difference in Mn₃O₄ nanoparticle size, size distribution, or morphology. This indicates that the more rapid introduction of reactants via the injection method does not cause a single nucleation event. Since there is a similar distribution of nanoparticle sizes in the standard and injection methods, we expect that the initial nucleation is not instantaneous in either case but continues with initial particle growth until the reactants are depleted upon a certain level. This is a marked contrast to formation of CeO₂ nanoparticles by aqueous HMT synthesis,²⁴ where nucleation

(22) Wu, P.-Y.; Pike, J.; Zhang, F.; Chan, S.-W. Low-Temperature Synthesis of Zinc Oxide Nanoparticles. *Int. J. Appl. Ceram. Technol.* **2006**, *3* (4), 272–278.

(23) Pike, J.; Chan, S.-W.; Zhang, F.; Wang, X.; Hanson, J. Formation of stable Cu₂O from reduction of CuO nanoparticles. *Appl. Catal. A* **2006**, *303*, 273–277.

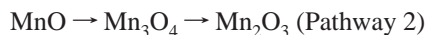
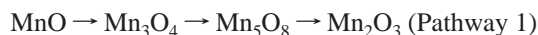
(24) Zhang, F.; Jin, Q.; Chan, S.-W. Ceria nanoparticles: Size, size distribution, and shape. *J. Appl. Phys.* **2004**, *95* (8), 4319–4326.

occurred as a single event at the beginning of the process, as indicated by a narrow size distribution of the ceria nanoparticles.

An increase in yield as the reaction temperature increases indicates that the temperature required for nucleation plays a significant role in the amount of product formed. By increasing the synthesis temperature, the number of particles nucleated increases, resulting in a higher Mn_3O_4 yield. With an increase in manganese nitrate concentration, more manganese ions are available, resulting in a larger quantity of Mn_3O_4 . The lower activation energy calculated for the lower nitrate concentration (0.02 M) condition suggests that the ratio of manganese ions to ammonium hydroxide produced from the dissociation of HMT also affects the reaction.

4.2. Mn_3O_4 Reduction. Mn_3O_4 nanoparticles reduce in 5% CO/95% He to form MnO nanoparticles, with smaller nanoparticles reducing at lower temperature than larger particles. This is expected in nanoparticle systems where kinetics are typically faster due to shorter diffusion distance and higher surface to volume ratio.

4.3. Mn_5O_8 Formation. Two different oxidation pathways are observed for MnO oxidation in 100% O_2 gas. MnO nanoparticles in the 14–18 nm size range oxidized according to Pathway 1, forming the intermediate phase Mn_5O_8 . Larger MnO nanoparticles (50 nm) and bulk MnO oxidized according to Pathway 2, which does not include formation of Mn_5O_8 as an intermediate



The critical size for formation of Mn_5O_8 in these conditions is between 18 and 50 nm. In Pathway 2 the Mn oxidation state increases from Mn^{+2} in MnO, to mixed-valence Mn_3O_4 [$(\text{Mn}^{+2})(\text{Mn}^{+3})_2\text{O}_3$], to Mn^{+3} in Mn_2O_3 . In Pathway 1 the net valence of the manganese ion increases from $\text{Mn}^{+2} \rightarrow \text{Mn}^{+2.67} \rightarrow \text{Mn}^{+3.2} \rightarrow \text{Mn}^{+3}$ to include the Mn_5O_8 [$(\text{Mn}^{+2})_2(\text{Mn}^{+4})_3\text{O}_8$] intermediate phase. Formation of Mn_5O_8 requires that oxidation of the Mn_3O_4 Mn^{+3} ions to Mn^{+4} precedes oxidation of the Mn_3O_4 Mn^{+2} ions. It is proposed that the higher surface area in the smaller nanoparticles allows for oxidation of the Mn_3O_4 octahedral Mn^{+3} ions preferentially over Mn^{+2} , perhaps by the presence of a higher concentration of surfaces containing the Mn^{+3} ions, which oxidize to Mn^{+4} and stabilize the Mn^{+2} ions. In this scenario for formation of Mn_5O_8 from Mn_3O_4 oxidation of Mn^{+3} to Mn^{+4} is more active than oxidation of Mn^{+2} to Mn^{+3} . As the particle size increases, oxidation of Mn^{+2} to Mn^{+3} becomes more active than oxidation of Mn^{+3} to Mn^{+4} , resulting in formation of Mn_2O_3 from Mn_3O_4 . Formation of an intermediate phase is also observed by in-situ TR-XRD in the reduction of CuO nanoparticles²³ with Cu_2O forming from reduction of CuO nanoparticles while bulk CuO reduces directly to Cu.

4.4. Mn_2O_3 Formation. Formation of Mn_2O_3 during oxidation required higher temperature for the 14–18 nm MnO particles than for the 50 nm MnO particles rather than the lower temperature oxidation observed in formation of

Mn_3O_4 . This suggests that interfacial energy acts as a barrier to nucleation and is responsible for the “sluggish” oxidation to Mn_2O_3 in smaller nanoparticles. The temperature of formation of Mn_2O_3 for the smaller nanoparticles is also greater than that required in the oxidation of bulk MnO. Bulk MnO particles formed Mn_2O_3 at temperatures 40–60 °C higher than formation of Mn_2O_3 from 50 nm MnO, indicating that in oxidation of these two sets of samples the kinetics are faster for smaller particles.

Oxidation of the smaller nanoparticles to Mn_2O_3 requires oxidation of the monoclinic Mn_5O_8 to cubic Mn_2O_3 , while cubic Mn_2O_3 forms directly from the tetragonal Mn_3O_4 when Mn_5O_8 is not formed as an intermediate phase. Earlier, we determined that formation of the interface acts as a barrier to nucleation of the reduced phase, making direct reduction to Cu less thermodynamically favorable than reduction to CuO to Cu_2O .²⁵

5. Conclusions

Nanoparticles of Mn_3O_4 ranging in size from 20 to 40 nm have been prepared by aqueous synthesis using HMT and manganese nitrate as precursors at temperatures between 22 and 80 °C. Synthesis temperature has a greater effect on the resulting nanoparticle size than manganese nitrate concentration or reaction time with particle size decreasing with increasing temperature. The most isotropic particles were obtained using a synthesis temperature of 50 °C. The yield of the reaction increases with increasing reaction temperature. Yield as a function of temperature is used to determine the activation energy of the reaction for 0.02 and 0.1 M manganese nitrate concentrations. Mn_3O_4 nanocrystals do not nucleate in a single event followed by particle growth; nucleation continues for a short while as initial growth occurs.

We use synchrotron radiation to perform in-situ TR-XRD ramping temperature reduction experiments to study reduction of Mn_3O_4 nanoparticle and oxidation of MnO nanoparticles. In reduction using 5% CO/He, smaller Mn_3O_4 nanoparticles reduced to MnO at lower temperature than larger nanoparticles and bulk Mn_3O_4 due to faster kinetics and shorter diffusion distance in the nanoscale system. Oxidation of MnO to Mn_3O_4 follows a similar trend with smaller MnO nanoparticles forming Mn_3O_4 at lower temperatures than larger MnO particles in 100% O_2 gas in ramping temperature.

The intermediate phase Mn_5O_8 is observed to form in the oxidation of MnO only in particles smaller than 18 nm and not from 50 nm MnO particles or bulk MnO oxidation. Formation of Mn_2O_3 from these smaller MnO nanoparticles requires greater temperature than that required to form Mn_2O_3 from bulk MnO, suggesting that nucleation of the new phase in very small, defect-free particles requires greater temperatures to overcome the excess surface or interfacial energy of the product particles.

Acknowledgment. J.P.’s effort was supported primarily by the MRSEC Program of the National Science Foundation under

(25) Pike, J.; Hanson, J.; Chan, S.-W. Surface energies of inter-phases formed in reduction of CuO nanoparticles. To be published.

Award Number DMR-0213574 and by the New York State Office of Science, Technology and Academic Research (NYS-TAR). J.P.'s effort was partially supported by Track 2, GK12: Technology Integration Partnership: Bringing Emerging STEM Research into Grades 5-12 enabled by New Technologies (NSF award 0338329). S.W.C.'s effort was primarily supported by the U.S. Department of Energy under DOE DE-FG02-05ER15730. Use of the National Synchrotron Light Source, Brookhaven National Laboratory, was supported by the U.S.

Department of Energy, Office of Science, Office of Basic Energy Sciences, under Contract No. DE-AC02-98CH10886. Research was carried out in part at the Center for Functional Nanomaterials, Brookhaven National Laboratory, which is supported by the U.S. Department of Energy, Division of Materials Sciences and Division of Chemical Sciences, under Contract No. DE-A C02-98CH10886.

CM071704B